Turkish Journal of Physics

http://journals.tubitak.gov.tr/physics/

Research Article

Turk J Phys
(2019) 43: 37 – 50

doi:10.3906/fiz-1804-14

Design and test of an apparatus for transient measurements of the thermal conductivity and volumetric heat capacity of solids

Florian GATHER[1], **Ekrem GÜNEŞ**[2,3,*], **Peter J. KLAR**[1]

[1]Institute of Experimental Physics I, Justus Liebig University Giessen, Giessen, Germany
[2]Institute of Inorganic and Analytical Chemistry, Justus Liebig University Giessen, Giessen, Germany
[3]Department of Alternative Energy Resources, Harran University, Şanlıurfa, Turkey

Received: 15.04.2018 • **Accepted/Published Online:** 04.01.2019 • **Final Version:** 22.02.2019

Abstract: Knowledge of the thermal conductivity (κ) of solids is crucial for all thermoelectric devices. A new approach in transient measurement to determine this value as well as electric conductivity (σ) and the Seebeck coefficient (S) is presented here. This approach can be combined with current steady-state methods. A cylindrical sample is mounted between two heat-flux sensors that can be heated or cooled at their outer ends. The input signals defining the heat fluxes at the sensors can be any arbitrary function of time, although some waveforms yield more valid results. The method is evaluated by employing a one-dimensional numerical model and finding the best fit to extract the thermal conductivity (κ) of the sample as well as its volumetric heat capacity ($c\rho$). Trial measurements on an insulating ($\sigma = 1 \times 10^{13}$ Sm^{-1}) and a conducting sample ($\sigma = 1 \times 10^{5}$ Sm^{-1}) are presented and the results are in good agreement with the literature and data obtained by a commercial laser-flash analysis system. Improvements in comparison to present measurement methods are the direct determination of κ compared to other transient methods like laser-flash analysis, shorter measurement times by acquiring $\kappa(T)$ data in a single temperature approach, and simultaneous S and σ measurements.

Key words: Thermal transport, steady-state measurement, dynamic measurement, ZT-meter

1. Introduction

Maximizing or minimizing heat transport plays a major role in many applications ranging from thermal isolation of buildings to microelectronics. Analyzing heat transport phenomena requires a distinction between radiation, convection, and conduction. The simultaneous occurrence of these three effects causes the slow and difficult nature of measurements of thermal conductivity. Thermal conductivity (κ) is an important material parameter, since, combined with the Seebeck coefficient (S) and electric conductivity (σ), it determines the thermoelectric figure of merit, $ZT = (S^2\sigma)/\kappa$, of materials [1–8]. All three values have to be determined first, in order to enhance performance in thermoelectric applications. Preferably all three measurements should be conducted in the same setup and in the same temperature cycle in order to minimize the degradation effects of the sample under test conditions [9,10]. While most current measurement systems support the simultaneous determination of S and σ, κ needs to be measured in a separate setup or a steady-state method, which slows down the whole procedure. Thus, the determination of κ creates a bottleneck in the characterization of thermoelectric properties.

*Correspondence: ekrem.guenes@anorg.chemie.uni-giessen.de

Transient methods of measuring thermal conductivity have turned out to be more reliable than steady-state approaches. Steady-state measurement techniques are usually based on the determination and analysis of a temperature profile across the sample [11,12]. The measurement times are rather long and the inherently large temperature gradient across the sample makes correction for convection and radiation effects rather difficult. Therefore, most of the modern measurement techniques are transient methods. New heat sources like laser or xenon flashes as well as lock-in techniques and new data logging methods are the basis for the more sophisticated transient measurement approaches used to date. These approaches can be divided into noncontact optical methods in which the heat input is controlled by light pulses, i.e. laser-/xenon-flash methods [13–15] or thermoreflectance-based [16–19] techniques and methods in which the heat input is delivered electrically by the Joule heating of a conductor, i.e. the 3ω method [20,21] and its predecessors: hot-wire and hot-plate methods [22].

It should be noted that all presently employed methods for measuring κ are performed at set sample temperatures. Temperature-dependent data of κ are not acquired during a continuous temperature run. This slows temperature-dependent measurements of κ down. Furthermore, all dedicated measurement approaches for determining κ are not compatible with simultaneous measurements of S and σ. The approach proposed here allows one to perform temperature runs, which speeds up the measurement time for acquiring $\kappa(T)$ data and is, in principle, compatible with Seebeck coefficient and electrical conductivity measurements, thus yielding a determination of temperature-dependent ZT data in one approach. The drawback is more elaborate data analysis though. However, this holds for almost all state-of-the-art approaches in which κ is extracted directly from the measurement data [18,19,23].

2. Experimental setup

The setup is designed such that there is a choice between three different measurement modi for determining κ. These comprise two conventional steady-state methods: the comparative mode and the guarded heater mode. In addition, it is possible to use a dynamic or transient mode, which is a transient method based on periodic heat inputs at the ends of the sample. The idea of this transient approach is to combine the advantages of steady-state methods, in particular the direct determination of thermal conductivity (κ), with those of dynamic methods, which have faster measurement times and the possibility of obtaining additional information on the product ($c\rho$) of specific heat capacity and mass density corresponding to a volumetric heat capacity. These improvements come at the cost of a more complex evaluation of the measurement data.

Figure 1 schematically depicts the main components of the setup used. A sample of cylindrical shape is embedded between two heat-flux sensors. Each consists of a glass cylinder with three embedded thermocouples (type K thermocouple consisting of chromel and alumel), which measure the temperatures along its axis. The diameters of the cylinders of the heat-flux sensors and that of the sample preferably should match for obtaining the best results. The innermost thermometers, T_3 and T_4, attached to the heat-flux sensors 1 and 2, respectively, also are in direct electric and thermal contact with the sample. The two heat-flux sensors are each connected to a separate heater, whose power input can be measured directly in 4-contact mode. The heaters 1 and 2 allow one to generate temperature gradients along the measurement bar. The setup is designed such that heater 1 may also be used in guarded heater mode. For this purpose, heater 1, on the one hand, has to be thermally insulated from its environment and, on the other hand, needs to be mounted onto the sensor in a mechanically stable way. These requirements are realized by using an additional heater as a guard heater mirroring the temperature of heater 1 and ensuring that heat flow from the heater is directed towards the sample. Heater 1 and its guard heater

are connected using plastic plates made out of polytetrafluoroethylene and a spring, allowing compensation for thermal expansion as well as serving as thermal insulation. The temperature difference between the guard heater and heater 1 is monitored by a thermocouple and serves as the input signal for the guard heater control.

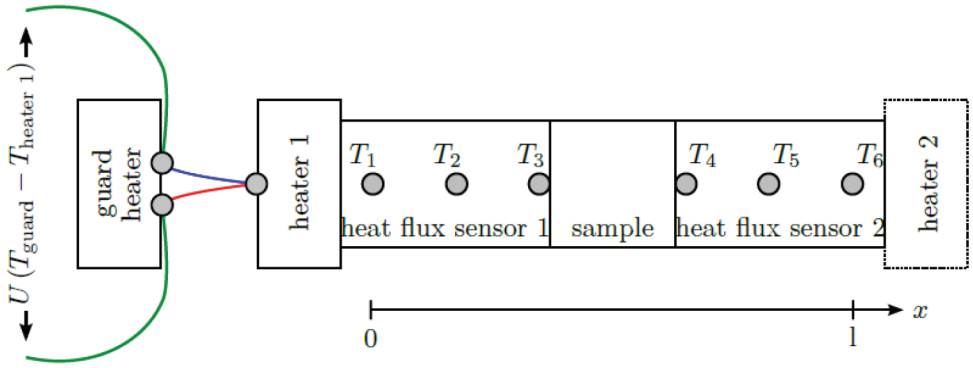

Figure 1. Schematic representation of the measurement setup. T_1 to T_6 denote thermocouples, which are used as thermometers. Another thermocouple is used between heater 1 and its guard heater to measure the temperature difference between them; the corresponding voltage output serves as input for the guard heater control. The entire setup is enclosed by heat shielding (not shown) and mounted onto a base plate (not shown) equipped with another heater and a cold finger to be able to access a temperature range between 100 K and 300 K.

In order to minimize radiation effects the whole measurement bar is surrounded by a copper shield reflecting thermal radiation from the sample back onto the sample and thus keeping radiative heat transport at a minimum. Moreover, ideally the temperature distributions of the shield and the measurement bar are equal, so that both are in thermal equilibrium and only radiative transport not perpendicular to the shield would influence the measurement. As the shielding consists of one material only, the ideal case requires the temperature distribution along the sample and along the heat-flux sensors to be linear. This requirement is fulfilled only if both have the same thermal conductivities. Thus, in general, for real measurements the ideal conditions are only approximately fulfilled. The whole measurement device is mounted on top of a base plate holding another heater system as well as a cold finger. It can be cooled by liquid nitrogen or liquid helium, allowing one to set and control the average temperature of the sample holder. A second radiation shield further minimizes the heat radiation to the environment, which is at ambient temperature.

3. Realization of steady-state measurements

A measurement in comparative mode can be conducted as follows. It is assumed that the thermal conductivity (κ_{sensor}) of the two heat-flux sensors is known. The temperature differences along the axis of the heat-flux sensors (e.g., $\Delta T = T_1 - T_2$ and $\Delta T = T_5 - T_6$) and along the axis of the sample (e.g., $\Delta T = T_3 - T_4$) are determined by the readings of the corresponding thermometers after a steady state has been reached. The gradients across the heat-flux sensors ($(\partial T/\partial x)_{sensor}$) and the sample ($(\partial T/\partial x)_{sample}$) are derived from these temperature differences and the distances between the corresponding thermometers. Assuming that the heat flow through the heat-flux sensors and the sample is the same, the thermal conductivity of the sample is derived by the following relationship:

$$\kappa_{sample} = \left(\frac{\partial T}{\partial x}\right)_{sensor} \cdot \kappa_{sensor} \left(\frac{\partial T}{\partial x}\right)^{-1}_{sample} \tag{1}$$

The variation in the power inputs of heaters 1 and 2 allow one to apply different temperature gradients. The readings of the additional thermocouples on the two heat-flux sensors offer the possibility to verify to what extent the assumption behind Eq. (1) is fulfilled, i.e. whether indeed the gradient across each of the sensors is constant and whether the temperature gradients across both sensors are the same. In comparative mode the use of the guard heater is optional.

The guarded heater mode is an absolute method based on knowledge of the heat flux through the sample. Power inputs of the guard heater and heater 1 are applied such that both heaters are kept at the same desired temperature (which is larger than that of heater 2). The guard heater and the heat shield surrounding the sample ideally should ensure that the thermal flux is unidirectional from heater 1 to heater 2 and in the steady state the power applied to heater 2 corresponds directly to the heat flux through the sample towards heater 2. The heat-flux density is given by $q = (I_{heater,1} \cdot U_{heater,1})/A$, where $I_{heater,1}U_{heater,1}$ is the power input of heater 1 in the steady state to keep the set temperature and A is the cross section of the sample. The temperature gradient across the sample is given by the temperature difference $\Delta T = T_3 - T_4$ divided by the known sample length L. Inserting these expressions into Fourier's law, the thermal conductivity of the sample can be calculated in a straightforward manner:

$$\begin{aligned} \kappa_{sample} &= -q \cdot \left(\frac{\partial T}{\partial x}\right)^{-1}_{sample} \\ &= \frac{I_{heater,1} \cdot U_{heater,1}}{A} \cdot \frac{L}{T_3 - T_4}. \end{aligned} \tag{2}$$

It is worth noting that measurements in comparative mode and guarded heater mode can be performed simultaneously during the same measurement cycle, allowing one to compare the corresponding results easily. Furthermore, the leads of the innermost thermocouples for measuring T_3 and T_4 may also be used as contacts for measuring the electric conductivity (σ) and the Seebeck coefficient (S). Thus, all three thermoelectric transport coefficients may be acquired in the same measurement run, which means the setup may also be used as a ZT-meter.

4. Realization of dynamic measurements

4.1. Conceptional ideas

Measurements of κ in dynamic or transient mode may be realized with the same setup. In addition to the sample's thermal conductivity (κ) its volumetric heat capacity ($c\rho$) is determined as well. The additional information about the volumetric heat capacity is contained in the time dependence of the temperatures T_1 to T_6.

As the analysis of the transient data is based on the solution of a differential equation, namely the heat equation, according to Eq. (3), the initial conditions of the problem need to be accurately defined in order to be specific and quantitative. In other words, a reliable evaluation of the temperature data and extraction of the material parameters of interest require that heat-flux sensors and the sample are in a known defined state at the beginning of the measurement. Different initial conditions may be anticipated; these can be either a steady state along the measurement bar consisting of the two heat-flux sensors surrounding the sample or a periodic oscillation in time of the state along the measurement bar. During the measurement heat fluxes from both sides of the sensor-sample arrangement will be used to vary the temperatures detected by the six thermometers. The correlation between heat flux as input and temperature variations as response is determined by the material

parameters of the measurement bar, in particular, the heat conductivities and heat capacities of both the sample and heat-flux sensors. Unfortunately, the heat flux cannot be determined directly by using the heater's power, since a guarding method might be too slow to handle fast temperature changes. Thus, the heat fluxes cannot be used as a boundary condition in the modeling required to extract the sample's thermal conductivity (κ) and volumetric heat capacity ($c\rho$). The temperature at each sensor is recorded as a function of time until no further information about the sample's properties can be gained from the measurements.

The volumetric heat capacity and thermal conductivity of the sample are extracted by fitting the measurement data to a numerical model of the heat-flux sensors and the sample. The model used in this work is based on the method of finite differences and uses the time-dependent temperatures measured at the two outermost thermocouples (T_1 and T_6) and the respective material parameters heat conductivity (κ) and volumetric heat capacity ($c\rho$) of the heat-flux sensors and the sample as input parameters. It facilitates the fitting procedure if the volumetric heat capacity and the thermal conductivity of the sensor material are known as a function of temperature. This represents no major obstacle, as these parameters are easily determined using a piece of sensor material instead of the sample, as in this case all three parts of the measurement bar are described by the same material parameters, and thus the number of free parameters in the fit is 2, similar to the case of a measurement bar with an arbitrary sample and known parameters for the sensor material. Therefore, we assume throughout the rest of the paper that the temperature-dependent material parameters of the sensor material are given and accurately known. In the fitting procedure the temperatures are calculated for discrete time steps on discrete grid points, are interpolated temporally and spatially to match the measurement conditions, and are compared with the measured values. The sum of the differences among all measurement points and the simulation results is defined as a cost function for an optimization algorithm and is minimized to obtain $c\rho$ and κ of the sample.

In the following, the numerical model, employed to calculate the temperature variations along the measurement bar, will be discussed. A number of methods exist to calculate the temperatures inside a one-dimensional homogeneous bar for different boundary conditions both analytically and numerically in the form of finite differences. When using the measured temperature data for the outermost sensors as input parameters of the model, the boundary condition is not an analytic expression; thus, a numerical model has to be employed.

The measurement bar typically consists of at least two different materials, i.e. that of the sensors and that of the actual sample. Therefore, it cannot be regarded as homogeneous. Some modifications of standard numerical methods have to be implemented to allow for inhomogeneous material parameters as well as nonuniform spatial discretizations. The latter is needed to enable one to perform calculations for arbitrary sample and sensor sizes. The starting point for the derivation of the model is the heat conduction equation:

$$c\left(x\right)\cdot p\left(x\right)\cdot\frac{\partial}{\partial T}T=\nabla\left[\kappa\left(x\right)\cdot\nabla T\left(x,\,t\right)\right] \tag{3}$$

By separating the spatial and temporal parameters one obtains an expression that can be discretized in two steps:

$$\frac{\partial}{\partial T}T(xt)=\frac{1}{c(x)\cdot p(x)}\cdot\nabla[\kappa(x)\cdot\nabla T(x,t)]$$

$$\frac{T_j^{m+1}-T_j^m}{\Delta T}=\frac{1}{c(x)\cdot p(x)}\cdot\nabla\left[\kappa(x)\cdot\frac{T_{j+0,5}^m-T_{j-0,5}^m}{\Delta x_{j,j+1}+\Delta x_{j,j-1}/2}\right] \tag{4}$$

$$\frac{1}{c_j \cdot p_j} \cdot \left[\kappa\left(x\right) \cdot \frac{2\kappa_{j,j+1} \cdot \left(T_{j+1}^m - T_j^m\right)}{\Delta x_{j,j+1} \cdot \left(\Delta x_{j,j+1} + \Delta x_{j,j-1}\right)} - \frac{2\kappa_{j-1,j} \cdot \left(T_j^m - T_{j-1}^m\right)}{\Delta x_{j-1,j} \cdot \left(\Delta x_{j-1,j} + \Delta x_{j,j+1}\right)} \right] \tag{5}$$

In Eq. (4) the temporal discretization was carried out by using the forward difference quotient, whereas in the case of spatial discretization a central difference quotient was applied. This constellation is often known as the forward-time central-space (FTCS) scheme; the temporal discretization is identical to the explicit Euler method. The continuous variables for the spatial coordinate x and the time t have been replaced by discrete positions j and points in time m. The distance between two neighboring grid points k, l is given by $\Delta x_{k,l}$ and the difference between two consecutive time steps by Δt. In the case of spatial discretization two temporary grid points are introduced, which are only used in the first derivation step. The definition of the variables and grid points is depicted in Figure 2. By approximating the second derivatives with respect to the position one obtains Eq. (5). The additional grid points cancel out and solving this equation for T_j^{m+1} leads to the conditional equation for the temperature at the grid point j at the next time step $(m+1)$.

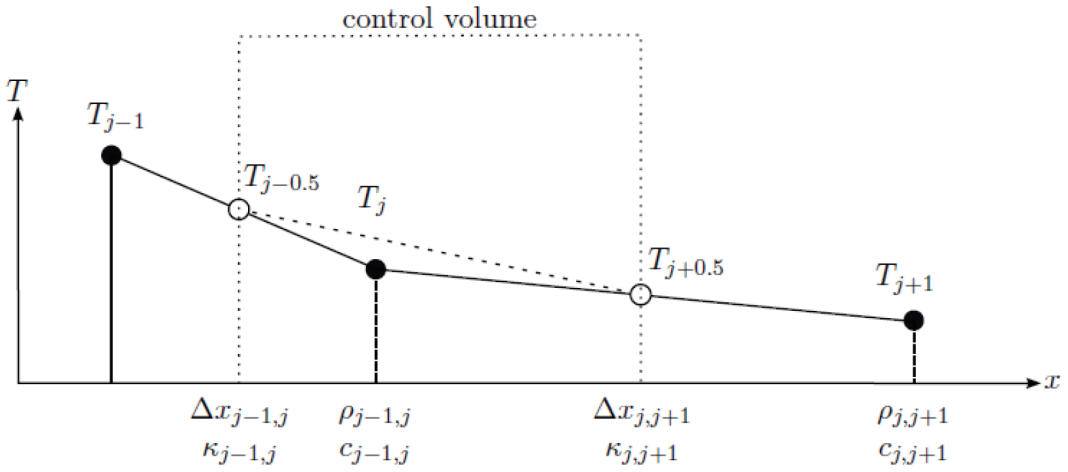

Figure 2. Scheme of the finite differences model used to solve the transient heat equation. Temperatures (T), heat capacities (c), and densities (ρ) are defined at the grid points; thermal conductivities κ are defined in between. Δx represents the distances between the points.

The temperatures are then calculated for all grid points and all time steps. As stated before, the initial conditions need to be known and the easiest way is to assume stationary conditions and obtain the initial temperatures by solving the stationary heat equation $= -\kappa \frac{\partial T}{\partial x}$.

For this purpose the two outermost temperatures are used again as boundary conditions. For time steps small enough the method is numerically stable. As an indication for the required time step length serves the following relationship [24]:

$$\frac{\kappa(x) \cdot \Delta t}{c(x) \cdot p(x) \cdot \Delta x^2} < \frac{1}{2}. \tag{6}$$

If this condition is not fulfilled, the FTCS scheme may yield unstable and oscillating solutions.

4.2. Measurement uncertainties for different excitation waveforms

As every real measurement is bound to have some degree of statistical uncertainty, the influence of measurement uncertainties of the thermometers T_1 to T_6 on the fitting results was investigated. To propagate the uncertainty from the temperature to the derived parameters a Monte-Carlo simulation was used, as proposed in Press et al. [25]. Here the measurement data are distorted with random artificial uncertainties and the fitting process is executed multiple times. The resulting distributions of κ and $c\rho$ are then analyzed and can lead to conclusions on the informational content of the measurement data.

Figure 3 depicts the results of a series of simulations in which the waveform of the exciting heater power was varied. Figures 3a and 3b show waveforms with a single and a double step, respectively, on one heater, while the temperature of the other remained unaffected. The next approach was to investigate sinusoidal excitation on one heater (Figure 3c), followed by simultaneous sinusoidal excitation on both heaters in an antiphase setup, which is shown in Figure 3d. The last investigated and depicted approach used two sinusoidal signals in phase and is shown in Figures 3e and 3f. Figures 3g and 3h visualize the values for κ and $c\rho$, respectively, related to the original parameters κ_0 and $c\rho_0$. The two-step functions show almost no difference in the results for κ. In contrast, the uncertainty of the $c\rho$ parameter is larger for two steps than for a single step. This is a direct result of the average sample temperature being larger in the latter case. Moreover, a deviation from the average Monte-Carlo result to the fit result without random noise being added can be observed. The deviation can be explained by the oscillation of the boundary temperatures of the numeric model.

In the case of the sine function on one boundary, while the temperature on the other was kept constant, the uncertainty of κ is comparable to those of the step functions. However, the uncertainty of the $c\rho$ parameter is smaller, since the information about the thermal heat capacity is gained during temperature changes. Using a sine function the temperature is changed over the complete measurement duration; thus the informational content concerning $c\rho$ is very large. However, if two sine functions are used in antiphase constellation, the values for $c\rho$show large deviations. In this case the heat flux through the sample is maximized and thus uncertainties with respect to κ are small. The temperatures inside the sample and the heat-flux sensors show nearly no phase shifts; thus the information on $c\rho$ is quite small and the corresponding uncertainty high. In the case of in phase excitation the net heat flow through the sample is zero. Thus, the error for κ is larger in this case, while, since the phase shifts are maximized, the uncertainties for $c\rho$ are small. The last wave form investigated, where a sine function was used for one end of the sample and the settling phase of the oscillation was considered, shows larger uncertainties in both parameters. This is, again, a direct result of the lower average temperatures in this case.

Based on this result, the mode where a sine was applied to one heater and the other heater is not used is considered to be the best approach, with regard to low uncertainties of the derived parameters κ and $c\rho$.

4.3. Transient measurements over wide temperature ranges

The transient measurement method wins over common steady-state methods due to the significant reduction of measurement times. Even in the case of transient measurements, each measurement requires a well-defined starting point, i.e. an accurate knowledge of the temperature distribution along the sample. This can be obtained intuitively by just waiting for the bar to establish a steady state. However, when it comes to temperature dependent measurements ($\kappa(T)$), this time-consuming equilibration procedure needs to be repeated for each temperature sampling point. In the following we describe an approach avoiding such long equilibration times in measurements of $\kappa(T)$. This approach is characterized by a continuous increase in base temperatures instead of a stepwise fashion, which means that the material parameters κ and $c\rho$ of the heat-flux sensors and the sample are changing during the course of the measurement.

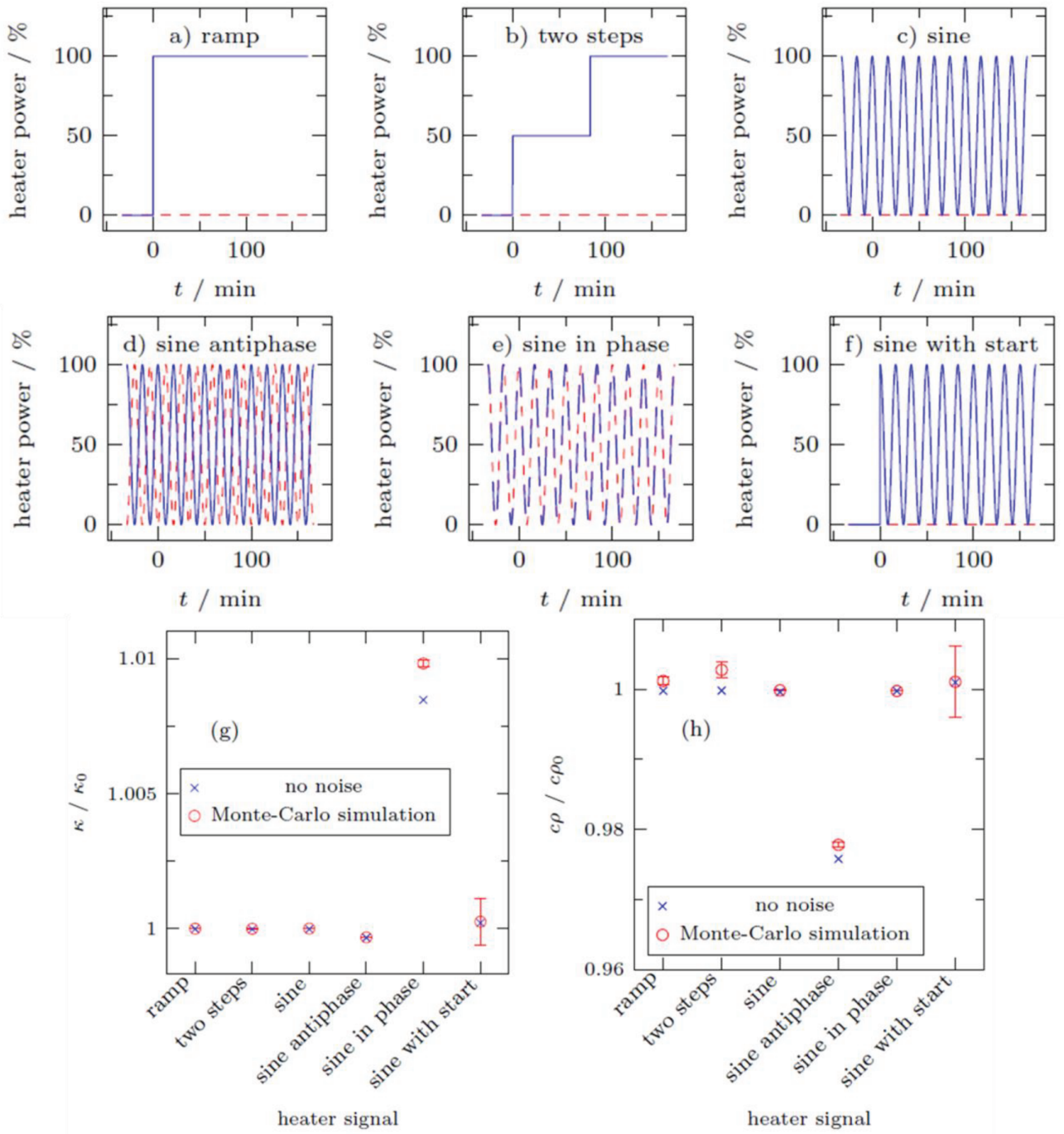

Figure 3. Comparison of different waveforms as heater inputs for the transient measurement mode. The solid lines are the input signals for heater 1, while the dashed lines represent those of heater 2. The uncertainties were determined with Monte-Carlo simulations. The simulations using the sine waveform as input show the smallest errors for $c\rho$. The first wave forms that were investigated were a single step (Figure 3a) and a double step (Figure 3b) on one heater, while the temperature of the other heater was kept constant. Next a sinusoidal excitation on one heater (Figure 3c), simultaneous sinusoidal excitation on both heaters (Figure 3d) in antiphase constellation, and one where two sinusoidal signals were used in phase (Figure 3e and 3f). Finally sinusoidal excitation was studied, which started at $t = 0$ instead of starting from a perfectly oscillating state. Figures 3g and 3h show the corresponding results for κ and $c\rho$, respectively, in relation to the original parameters κ_0 and $c\rho_0$.

In principle, temperature-dependent parameters can be implemented in a numerical model; nevertheless, the complete fitting of a measurement over a large temperature range in a single run of the current fitting procedure remains challenging and turns out to be too complex. Since the overall measurement time is probably longer than the time needed for a single measurement step at a constant base temperature, the computation time for a single calculation of χ^2 rises as more measurement time has to be covered. Additionally, the number of simulations needed to complete the fit procedure also increases when the parameters of the sample are described by a piecewise interpolation between several nodes. This in turn increases the number of fit parameters.

Figure 4 illustrates an alternative approach to evaluate the data, which will yield more reliable results. At first the input data are organized by division into several intervals (p_n). For each interval, the average sample temperature T_n is determined. Subsequently each interval is fitted to the numerical model assuming that κ and $c\rho$ of the sample are temperature independent. The final temperature distribution of the simulation of the preceding interval is used as a starting point for all simulations succeeding the first interval. This method yields values for κ_n and $c\rho_n$ that are quite accurate within their respective interval p_n; on the other hand, these values are still prone to errors due to the assumption of a constant κ and $c\rho$. To improve the accuracy another, third step is performed, in which each interval p_n is fitted again, now using temperature-dependent values for κ and $c\rho$, which are piecewise linearly interpolated between κ_{n-1}, κ_n, κ_{n+1} and $c\rho_{n-1}$, $c\rho_n$, $c\rho_{n+1}$, respectively. After several iterations of this step the resulting parameters will converge in a self-consistent manner and the resulting curves can eventually be refined by adding intermediate grid points into the piecewise interpolation of κ and $c\rho$. One has to be cautious that the number of grid points is not too large, as a certain number of measured temperatures is required at each κ or $c\rho$ point for an accurate determination of the values. Another iteration, repeating step 3, has to be conducted after the insertion of additional grid points.

Figure 5 shows the results of an evaluation process as described above. Input data have been generated with the help of COMSOL (Multiphysics Modeling Software) (downloaded from https://www.comsol.de/) utilizing temperature-dependent thermal properties of the sample and the heat-flux sensors. The thermal parameters of the sensors therefore were presumed to be known. The use of sinusoidal heater power by heater 1 increases the sensitivity towards the $c\rho$ parameter. The base temperature undergoes a linear increase from 100 K to 300 K. Figure 5a depicts the temperatures of the six thermometers as a function of time; Figures 5b and 5c illustrate the fitted values for κ and $c\rho$, respectively, at different stages of the evaluation process. It is shown that the use of temperature independent κ and $c\rho$ in the first step leads to deviations from the original values κ_0 and $c\rho_0$. However, after performing steps 2 to 4, both parameters converge nicely towards the original values.

As mentioned above, this approach enables large savings in time due to the absence of time-consuming waiting periods and the possibility to yield data over the course of the whole temperature sweep. Without this approach, the necessary waiting time of 5 h in the steady-state measurements of this work is demanded at each base temperature for the system to equilibrate. This illustrates the tremendous benefit delivered by our continuous approach, since those times are omitted completely (with exception of the first data point). Furthermore, the continuous measurement allows for a finer temperature resolution of the extracted material parameters.

The price to pay is somewhat heavier, but with manageable computational duties in the data analysis. The fitting of the data depicted in Figure 5 took 15 min on a desktop processor using a single CPU core.

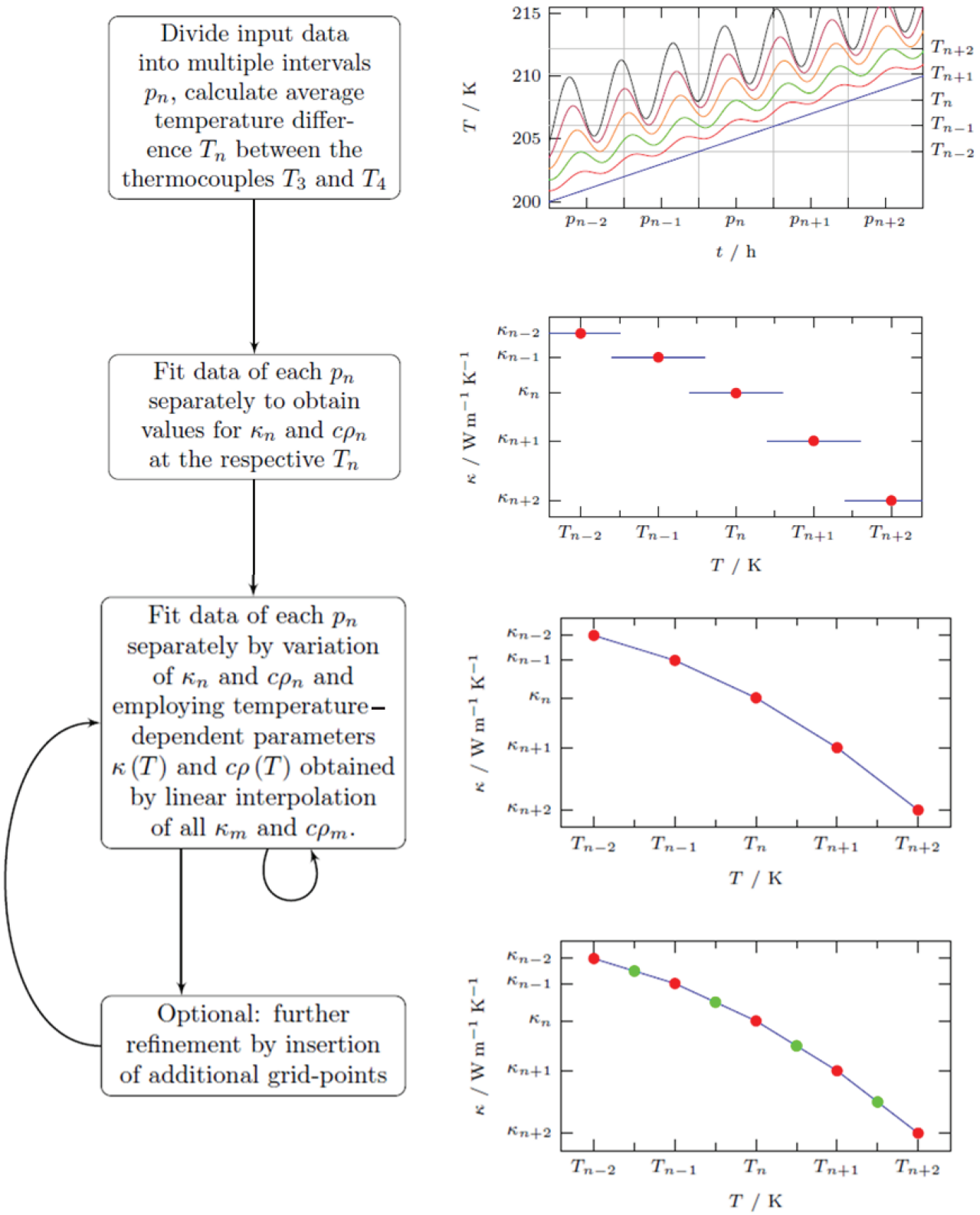

Figure 4. Flow chart for the evaluation process for measurements over a large temperature range with temperature-dependent thermal properties of the sample and heat-flux sensor material.

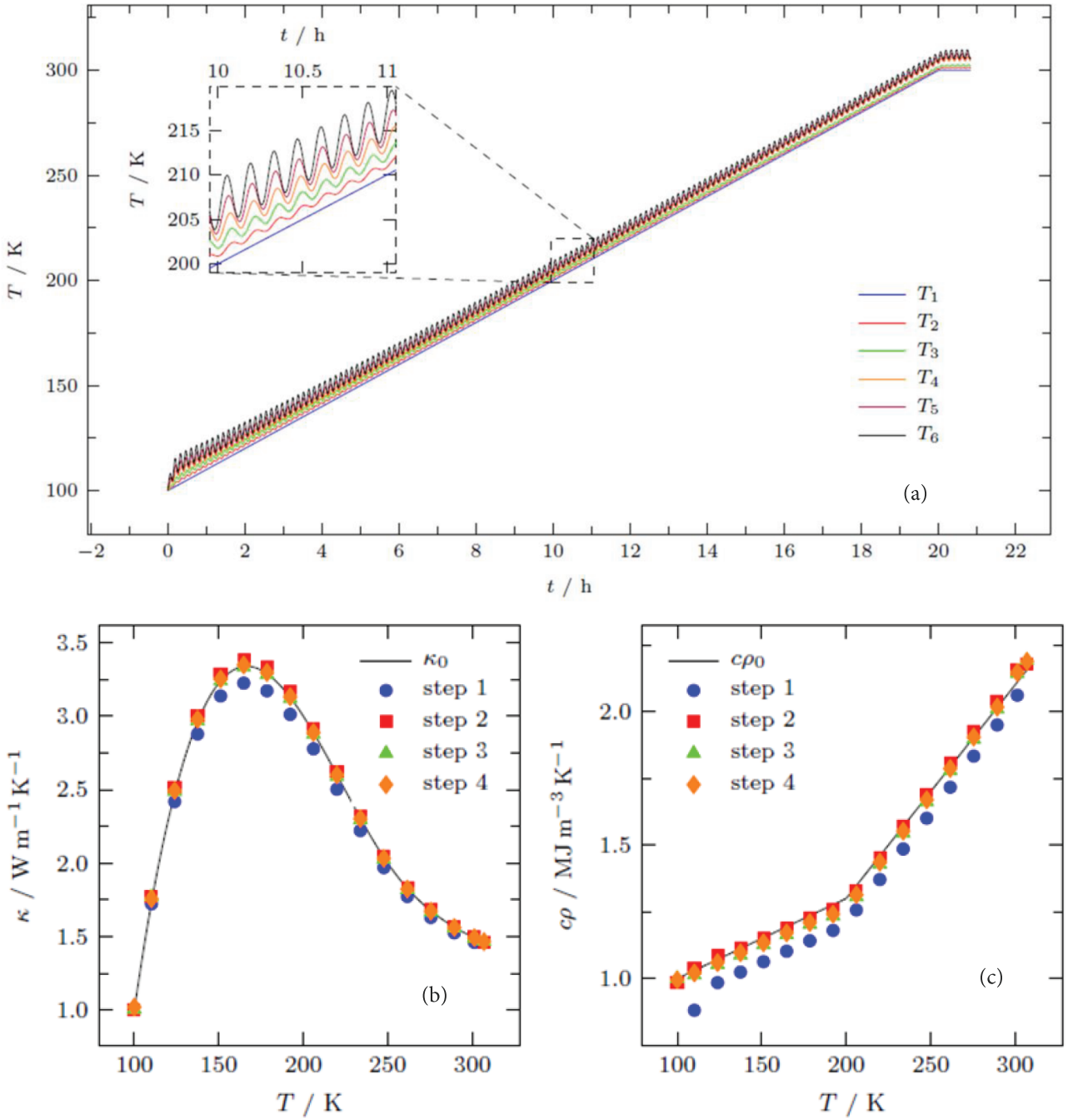

Figure 5. In (a) the simulated temperatures for a measurement without a constant base temperature are shown. (b) and (c) depict the corresponding results for κ and $c\rho$ of the sample obtained with the evaluation method shown in Figure 4.

5. Experimental results

First experiments using the new transient measurement show that the novel transient approach indeed works. The material parameters κ_{sensor} and $(c\rho)_{sensor}$ of the sensor were determined by a separate measurement employing the 3ωmethod and were used as fixed parameters in the analysis of the measurements described below.

Figure 6 depicts the results of a measurement on a polyoxymethylene (POM) sample of low electrical conductivity (typical values are of the order of $\sigma = 1 \times 10^{-13}$ Sm^{-1}) [26] by the transient method as well as by the two steady-state methods. The data show that for higher temperatures the results of the guarded heater method deviate from those obtained by the other methods. This might be a result of radiation effects and parasitic heat currents. Especially with low conducting samples, such as the POM sample, the impact of parasitic currents on the guarded heater method is expected to be large. Figure 6a shows that the results of the comparative approach and the transient approach are in good agreement with each other. The literature value for κat 280 K of POM according to a datasheet (provided by www.hpceurope.com) is somewhat lower. Unfortunately, as there are different types of POM, it is not possible to decide whether this discrepancy between values of about 30% is due to material issues, e.g., different material morphology, or an instrumental issue. Figure 6b shows the corresponding values for the volumetric heat capacity ($c\rho$), obtained by analysis of the data of the same temperature sweep in transient mode. In this case, the results of the transient measurement agree very well with temperature dependent data from another reference in the literature [26].

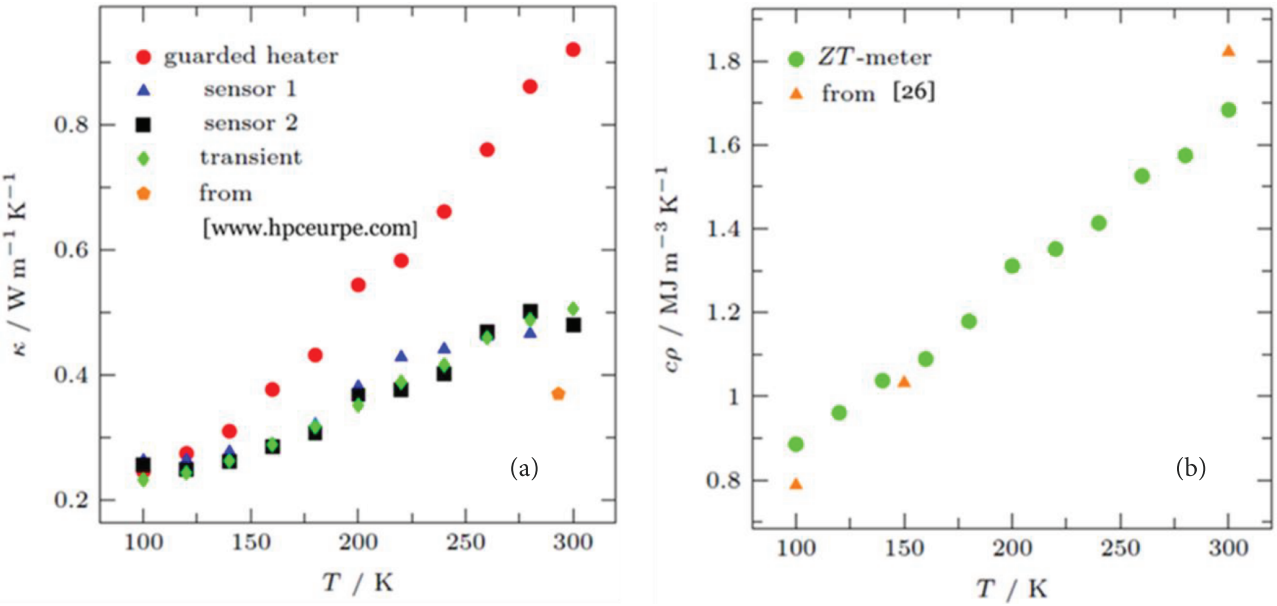

Figure 6. Measurement results for a polyoxymethylene (POM) sample in the temperature range from 100 K to 300 K. (a) Thermal conductivity measured with the three different modes, i.e. comparative, guarded heater, and transient mode. Sensor 1 and sensor 2 denote the measurements in comparative mode based on the data of the corresponding sensor. (b) Values of the volumetric heat capacity extracted in the same transient measurement sweep and corresponding data from the literature.

In a second experiment the thermal properties of a bismuth–antimony alloy ($Bi_{0.8}Sb_{0.2}$) sample were investigated. The sample was prepared by cold pressing from ball-milled nanoparticles followed by a sintering step and exhibited an electrical conductivity of about 2×10^5 Sm^{-1} at ambient temperature [27]. A temperature sweep in transient mode was performed and the corresponding results for κ and $c\rho$ are depicted in Figure 7. In the case of such an almost metallic, thermally well conducting sample the uncertainty of the measurement result is determined mainly by the accuracy achieved in the temperature measurements. Figure 7a shows that the results of the guarded heater method are in better agreement with those of the other methods than in case of the POM sample. However, the values obtained in comparative mode and transient mode show larger relative deviations than those obtained by the same methods from the POM sample.

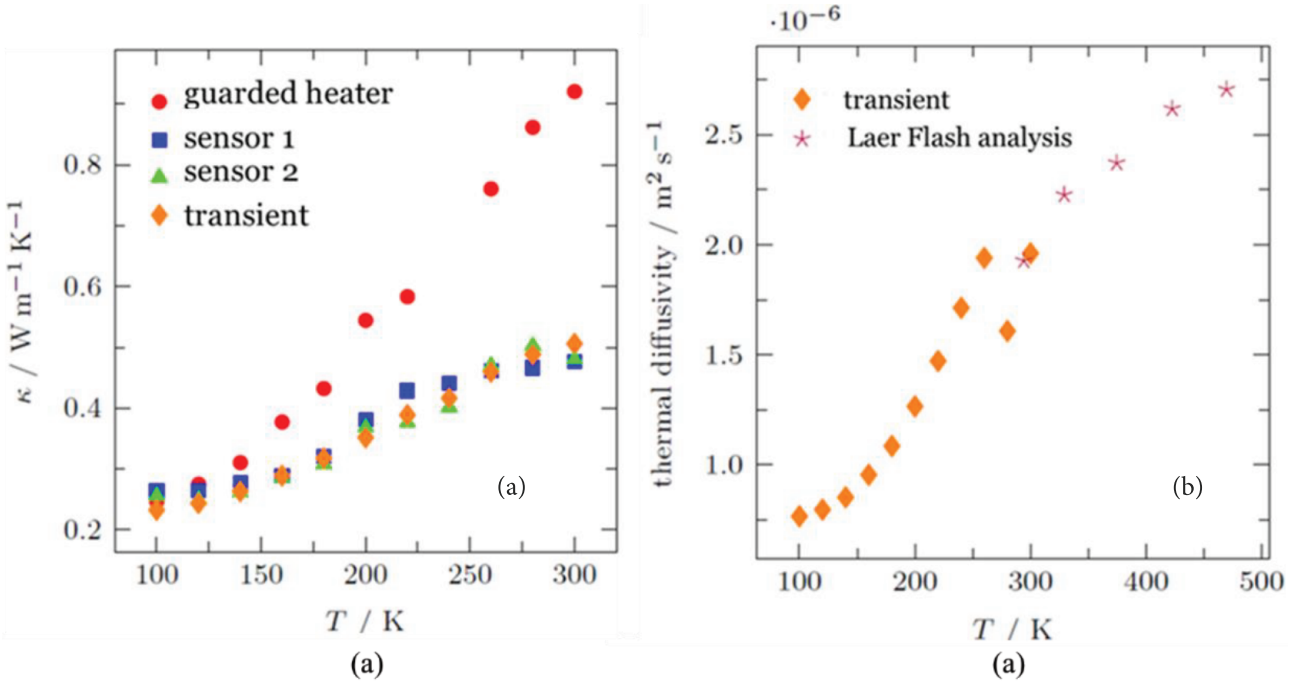

Figure 7. Results of temperature-dependent measurement of a $Bi_{0:8}Sb_{0:2}$ sample. (a) Thermal conductivity measured with the three different modes, i.e. comparative, guarded heater, and transient mode. Sensor 1 and sensor 2 denote the measurements in comparative mode based on the data of the corresponding sensor. (b) Values of the volumetric heat capacity extracted in the same transient measurement sweep (100 K to 300 K) and values extracted by a laser-flash analysis of the same sample (300 K to 500 K).

Also shown in Figure 7b are results for the thermal diffusivity of the same $Bi_{0:8}Sb_{0:2}$ sample obtained by a commercial laser-flash analysis setup. However, the measurements could only be performed in different temperature ranges, i.e. the transient mode measurements in the low temperature range from 100 K to 300 K and the laser-flash analysis in the higher temperature range from 300 K to 500 K. The data at 300 K are in reasonable agreement and the temperature-dependent trends within the two sets of data points agree well.

6. Conclusion

We have presented a novel measurement setup for transient measurements of the thermal conductivity (κ) and the volumetric heat capacity ($c\rho$) of bulk materials. The roots of this transient measurement approach date back as far as 1822, when Fourier suggested using sinusoidal heating as the boundary condition at one end of a sample in experiments for quantitative determination of thermal material properties. Refining this approach, in particular by employing efficient numerical algorithms and data management in the analysis, allows us to propose a fast measurement procedure in which temperature-dependent data $\kappa(T)$ and $c\rho(T)$ may be obtained in a single continuous temperature sweep, avoiding long equilibration times during the entire measurement. The uncertainties of the measurement technique were estimated by Monte-Carlo simulations and the first experiments demonstrated the suitability of the approach for samples in a wide range of electric conductivities. Furthermore, the setup is designed in such a way that, in addition to transient measurements, also steady-state measurements of κcan be performed in comparative mode or guarded heater mode. In principle, the measurement bar containing the sample allows simultaneous measurements of the sample's Seebeck coefficient (S) as well as its electrical conductivity (σ) in the same measurement run as for κ, and thus the setup has the potential to be extended to a ZT-meter.

References

[1] Farahi, N.; Prabhudev, S.; Bugnet, M.; Botlon, G. A.; Zhao, J.; Tse, J.; Salvador, J. R.; Kleinke, H. *RSC Adv.* **2015**, *5*, 65328-65336.

[2] Ge, Z. H.; Zhao, L. D.; Wu, D.; Liu, X.; Zang, B. P.; Li, J. F.; He, J. *Mater. Today* **2016**, *19*, 227-239.

[3] Güneş, E.; Landschreiber, B.; Hartung, D.; Elm, M. T.; Rohner, C.; Klar, P. J.; Schlecht, S. *J. Electron. Mater.* **2014**, *43*, 2127-2133.

[4] Zhang, X.; Zhao, L. D. *Journal of Materiomics* **2015**, *1*, 92-105.

[5] Güneş, E.; Landschreiber, B.; Homm, G.; Wiegand, C.; Tomes, P.; Will, C.; Elm, T. M.; Paschen, S.; Klar, P. J.; Schlecht, S. et al. *J. Electron. Mater.* **2018**, *47*, 6007-6015.

[6] Tan, G.; Zhao, L. D.; Kanatzidis, M. C. *Chem. Rev.* **2016**, *116*, 12123-12149.

[7] Zhang, R. Z.; Gucci, F.; Zhu, H.; Chen, K.; Reece, M. J. *Inorg. Chem.* **2018**, *57*, 13027-13033.

[8] Tang, G.; Yang, W.; Wen, J.; Wu, Z.; Fan, C.; Wang, Z. *Ceram. Int.* **2015**, *41*, 961-965.

[9] Güneş, E.; Gundlach, F.; Elm, T. M.; Klar, P. J.; Schlecht, S.; Wickleder, S. M.; Müller, E. *ACS Appl. Mater. Interfaces* **2017**, *9*, 44756-44765.

[10] Güneş, E.; Wickleder, S. M.; Müller, E.; Elm, T. M.; Klar, J. P. *AIP Advances* **2018**, *8*, 075319.1-075319.6.

[11] Lees, C. H. *Phil. Trans. R. Soc. Lond. A* **1898**, *191*, 399-440.

[12] Poensgen, R. *Mitteilungen über Forschungsarbeiten auf dem Gebiete des Ingenieurwesens*; Springer-Verlag: Berlin, Germany, 1912.

[13] Parker, W. J.; Jenkins, R. J.; Butler, C. P.; Abbott, G. L. *J. Appl. Phys.* **1961**, *32*, 1679-1684.

[14] Vözar, L.; Hohenhauer, W. *Int. J. Thermophys.* **2005**, *26*, 1899-1915.

[15] Hay, B.; Filtz, J. R.; Hameury, J.; Rongione, L. *Int. J. Thermophys.* **2005**, *26*, 1883-1898.

[16] Paddock, C. A.; Eesley, G. L. *J. Appl. Phys.* **1986**, *60*, 285-290.

[17] Rosencwaig, A.; Opsal, J.; Smith, W. L.; Willenborg, D. L. *Appl. Phys. Lett.* **1985**, *46*, 1013-1015.

[18] Liu, J.; Zhu, J.; Gu, X.; Schmidt, A.; Yang, R. *Rev. Sci. Instr.* **2013**, *84*, 034902.1-034902.3.

[19] Schmidt, A. J.; Cheaito, R.; Chiesa, M. *Rev. Sci. Instr.* **2009**, *80*, 094901.1-094901.9.

[20] Cahill, D. G.; Pohl, R. O. *Phys. Rev. B* **1987**, *35*, 4067-4073.

[21] Gahill, D. G. *Rev. Sci. Instr.* **1990**, *61*, 802-808.

[22] Gustafsson, S. E.; Karawacki, E.; Khan, M. N. *J. Phys. D: Appl. Phys.* **1979**, *12*, 1411-1421.

[23] Kim, J. H.; Feldman, A.; Novotny, D. *J. Appl. Phys.* **1999**, *86*, 3959-3963.

[24] Çengel, Y. A. *Heat Transfer: A Practical Approach*, 2nd ed.; McGraw-Hill: New York, NY, USA, 2002.

[25] Press, W. H.; Teukolsky, S. A.; Vetterling, W. T.; Flannery, B. P. *Numerical Recipes in C: The Art of Scientific Computing*, 2nd ed.; Cambridge University Press: New York, NY, USA, 1992.

[26] Lüftl, S.; Visakh, P. M.; Chandran, S. *Polyoxymethylene Handbook: Structure, Properties, Applications and Their Nanocomposites*; John Wiley & Sons, Inc.: Hoboken, NJ, USA, 2014.

[27] Will, C. H.; Elm, M. T.; Klar, P. J.; Landschreiber, B.; Güneş, E.; Schlecht, S. *J. Appl. Phys.* **2013**, *114*, 193707.1-193707.7.